ELECTRICAL RESISTIVITY MEASUREMENTS ON THE ROSS ICE SHELF*

By CHARLES R. BENTLEY

(Department of Geology and Geophysics, University of Wisconsin, Lewis G. Weeks Hall, Madison, Wisconsin 53706, U.S.A.)

ABSTRACT. Electrical resistivity measurements were made along two perpendicular profiles on the Ross Ice Shelf, Antarctica, in 1973–74. Apparent resistivities are generally well determined at electrode separations from 10 m out to 600 m, where the effect of the highly conducting sea-water beneath the shelf becomes strongly felt. Schlumberger and equatorial-dipole data are in excellent agreement on each profile; apparent resistivities on the two profiles, however, differ by about 12% at separations greater than about 30 m. This apparent anisotropy is attributed to a presumed inhomogeneity at a few tens of meters depth, rather than to true anisotropy in the bulk resistivity.

A computer program has been developed to calculate apparent resistivities on an ice shelf in which the density and temperature, and thus the resistivity, vary continuously with depth. Temperatures have been calculated according to the analysis of Crary (1961[b]) for a steady-state ice shelf; densities have been calculated from seismic velocity data. Several different models of the dependence of resistivity on density have been tested—one appears to fit the observations very closely, but it must be accepted only with great caution because the assumptions on which it is based are violated in the ice shelf.

The activation energy and the rate of bottom melting or freezing upon which the temperature–depth variations depend have been treated as variable parameters in the modeling. The most satisfactory model corresponds to a melt/freeze rate close to zero, and an activation energy, 0.25 eV (24 kJ mol⁻¹), in agreement with laboratory measurements on Antarctic ice samples, although less than that suggested by previous field measurements. However, since the actual temperatures in the ice shelf are unknown, models that combine a substantial melt rate with a higher activation energy, or a substantial freeze rate with a lower activation energy, cannot be ruled out at present. Future measurements in places where the temperature profile is known should resolve this uncertainty.

The actual resistivity in the solid ice at a depth of about 100 m (temperature about −23°C), lies within ±10% of 70 000 Ωm, thus once again confirming the very low resistivities typical of polar glacial ice. The resistivity is, in fact, only about half that found near Roosevelt Island to the north and "Byrd" station to the east. That difference is believed to be real, but its cause is not known and probably will not be known until the basic cause for the generally low resistivity of polar ice is better understood.

RÉSUMÉ. *Mesures de résistivité électrique dans le Ross Ice Shelf.* Des mesures de résistivité électrique ont été faites selon deux profils perpendiculaires dans le Ross Ice Shelf en Antarctique, en 1973–74. Les résistivités apparentes sont, en général, bien déterminées pour des distances entre électrodes allant de 10 à 600 m, distance à laquelle l'influence de l'eau de mer conductrice sous la calotte devient très sensible.

Les données de l'appareil Schlumberger et du dipole équatorial concordent très bien dans chaque profil; les résistivités apparentes des deux profils cependant diffèrent d'environ 12% pour des distances entre électrodes supérieures à environ 30 m. Cette anisotropie apparente est attribuée à une inhomogénéité présumée à quelques dizaines de mètres de profondeur plutôt qu'à une véritable anisotropie dans la résistivité de la masse.

Un programme sur ordinateur a été élaboré pour calculer les résistivités apparentes d'une calotte de glace dans laquelle densité et température, et donc la résistivité, varient de manière continue avec la profondeur. Les températures ont été calculées d'après l'analyse de Crary (1961[b]) pour une calotte en état d'équilibre; les densités ont été calculées à partir des vitesses déterminées par la sismique.

On a essayé plusieurs modèles différents pour la loi qui fait dépendre la résistivité de la densité. L'un d'eux semble s'ajuster fort bien avec les observations mais on ne doit l'admettre qu'avec beaucoup de précautions parce que les hypothèses sur lesquelles il repose ne sont pas réalisées dans la plateforme.

L'énergie d'activation et les vitesses de fusion ou de regel à la base de la plateforme dont dépendent les variations de la température en fonction de la profondeur ont été traitées dans la modèlisation comme des paramètres indépendants. Le modèle le plus satisfaisant correspond à une vitesse de fusion ou regel proche de zéro et à une énergie d'activation de 0,25 eV (24 kJ mol⁻¹), en conformité avec les mesures en laboratoires sur des échantillons de glace arctique, quoique moindre que celle suggérée par de précédentes mesures de terrain. Cependant puisque les températures réelles dans la calotte sont inconnues, les modèles qui prennent en compte une forte vitesse de fusion avec une plus forte énergie d'activation, ou une forte vitesse de regel avec une plus faible énergie d'activation, ne peuvent pas être rejetés pour le moment. Durant la saison 1976–77 les mesures de résistivité seront faites à proximité d'un sondage dans la calotte où les températures seront connues, ce qui nous donnera une meilleure connaissance de l'énergie d'activation et, par conséquent, de l'effet de la densité. Des mesures ultérieures en d'autres emplacements pourront alors fournir des températures avec une précision de un à deux degrés, et conduire, si la plateforme est en état d'équilibre, à une précision de peut-être ±0,1 m/an dans l'estimation des vitesses de fontes et de regel à la base. Si la plateforme n'est pas en état d'équilibre, les mesures de résistivité peuvent, espère-t-on, déboucher sur un modèle valable du changement en cours.

15

La résistivité réelle dans la glace solide à une profondeur d'environ 100 m (température de l'ordre de −23°C) est, à 10% près de 70 000 Ω m ce qui confirme à nouveau les très basses résistivités qui caractérisent la glace des glaciers polaires. La résistivité est, en fait, seulement la moitié de celle trouvée près de Roosevelt Island au Nord de la station "Byrd" à l'Est. On pense que cette différence est bien réelle mais son explication n'est pas connue et ne sera probablement pas connue tant que la raison profonde de la faiblesse de la résistivité de la glace polaire ne sera pas mieux comprise.

ZUSAMMENFASSUNG. *Messungen des elektrischen Widerstandes auf dem Ross Ice Shelf.* Entlang zweier senkrecht zueinander verlaufenden Profile auf dem Ross Ice Shelf wurden im Sommer 1973–74 elektrische Widerstands-messungen vorgenommen. Scheinbare Widerstände lassen sich im allgemeinen bei Elektrodenabständen von 10 m bis zu 600 m gut bestimmen; bei grösseren Auslagen macht sich der Einfluss des hoch leitfähigen Meerwassers unter dem Schelf stark bemerkbar. Daten von Schlumberger- und Äquatorial-Dipolen stimmen bei jedem Profil ausgezeichnet überein; doch weichen die scheinbaren Widerstände um etwa 12% bei Auslagen von mehr als 30 m voneinander ab. Diese scheinbare Anisotropie ist eher der anzunehmenden Inhomogenität bis zu einer Tiefe von einigen Dekametern zuzuschreiben als einer wirklichen Anisotropie im Gesamtwiderstand.

Zur Berechnung des scheinbaren Widerstandes auf Schelfeisen wurde ein Computer-Programm entwickelt, in dem Dichte und Temperatur, und damit der Widerstand, kontinuierlich mit der Tiefe variieren. Die Temperaturen wurden entsprechend der Analyse von Crary (1961[b]) für ein stationäres Schelfeis berechnet; die Dichten wurden aus seismischen Geschwindigkeitsdaten hergeleitet. Verschiedene Modelle für die Beziehung zwischen Widerstand und Dichte wurden geprüft, von denen eines sehr gut zu den Beobachtungen zu passen scheint; doch muss es mit allem Vorbehalt betrachtet werden, weil die Annahmen, auf denen es beruht, im Schelfeis nicht zutreffen.

Die Aktivationsenergie und das Ausmass des Schmelzens oder Anfrierens am Untergrund, wovon die Änderung der Temperatur mit der Tiefe abhängt, wurden als variable Parameter in das Modell eingeführt. Das am meisten befriedigende Modell entspricht einer Abschmelz/Gefrierrate von nahezu Null und einer Aktivationsenergie von 0,25 eV (24 kJ mol⁻¹), was mit Labormessungen an antarktischen Eisproben übereinstimmt, jedoch unterhalb der Annahmen aus früheren Feldmessungen liegt. Da jedoch die tatsäch-lichen Temperaturen im Schelfeis unbekannt sind, können Modelle, die eine beträchtliche Schmelzrate mit einer höheren Aktivationsenergie oder eine wesentliche Gefrierrate mit einer geringeren Aktivations-energie kombinieren, derzeit nicht ausgeschlossen werden. Zukünftige Messungen an Stellen wo das Tem-peraturprofil bekannt ist sollten diese Ungewissheit lösen.

Der tatsächliche Widerstand im festen Eis bei einer Tiefe von etwa 100 m (Temperatur *c.* −23°C) liegt mit einer Schwankungsbreite von 10% bei 70 000 Ω m, womit erneut die für polares Gletschereis typischen sehr niedrigen Widerstandswerte bestätigt werden. Der Widerstand ist tatsächlich nur etwa halb so gross als der nahe von Roosevelt Island nach Norden und bei der "Byrd"-Station nach Osten gemessene. Dieser Unterschied ist als reell zu betrachten, doch ist seine Ursache unbekannt und wird es vermutlich auch bleiben, bis der tiefere Grund für den generell niedrigen Widerstand von polarem Eis besser verstanden wird.

INTRODUCTION

Electrical resistivity measurements on ice shelves are very rare. Prior to the present work, only two such profiles had been completed, the first near Roosevelt Island (Hochstein, 1967), the second on the McMurdo Ice Shelf (Hochstein and Risk, 1967). But the McMurdo Ice Shelf is thin, has a regime quite different from that of the Ross Ice Shelf, and is modified by brine soaking within the ice column. Thus the usefulness of resistivity studies, strongly suggested by Hochstein's earlier work, remained untested.

The measurements reported on here were made as part of the ongoing Ross Ice Shelf Geophysical and Glaciological Survey (RIGGS), a survey of the entire Ross Ice Shelf that includes measurements of ice thickness and surface strain-rates. The parent Ross Ice Shelf Project (RISP) will, from a program of drilling through the ice, yield well-determined values of density and temperature as a function of depth. Resistivity measurements have been undertaken as an opportunity to take advantage of these known parameters to learn more about the electrical characteristics of Antarctic firn and ice, and the effect of possible bottom melting or freezing on resistivity profiles. The initial resistivity profiles reported on in this paper were carried out where a number of other geophysical and glaciological measurements yielding reasonably accurate density–depth information were made, but not at a present (or probable future) drill site. Temperatures are thus unknown. The observations have therefore been compared with resistivities to be expected on the basis of calculated temperature–depth curves. The analysis leads to a good determination of the actual resistivity, rather broad limitations on acceptable values of the activation energy and the bottom melt/freeze rate, and a fair insight into the possible resolving power of resistivity profiling when appropriate temperature models are better known.

FIELD MEASUREMENTS

The resistivity soundings were made near the RIGGS I base camp (station BC) in late December 1973 and January 1974. Measurements were made along two perpendicular lines, called Profile A and Profile B, with a common center; Profile A (Fig. 1) was taken along the direction to station J9 (the initial RISP drill site), roughly parallel to the direction of ice flow. Measurements were made using both Schlumberger and equatorial-dipole arrays (Fig. 2), the results of which should be nearly identical for a simple one-dimensional variation of resistivity in the ice, that is, a resistivity which varies only as a function of depth. The lines were extended to a maximum separation (*a* in Fig. 2) of approximately 600 m along each profile.

The current source was a bank of 45 V dry cells, producing a maximum of 810 V. 1.2 m copper rods were used for both current and potential electrodes at larger spacings; nails were used instead at short spacings to maintain a satisfactory ratio of spacing to electrode depth. Experiments were made with multiple electrodes in an attempt to reduce the electrode contact resistance, but these were not very successful. The best success in reducing contact resistance was gained by soaking the firn surrounding the electrode with salt water. Potentials were measured with a Keithley model 600A electrometer, having an input impedance of 10^{14} Ω. No absolute calibration of the electrometer was possible during the actual measurement, but comparisons with an electronic voltmeter and two cathode-ray oscilloscopes in the base-camp laboratory all showed agreement within 5%. Copper wire with a very high-resistance insulation, of the same type used for resistivity measurements on land, was employed.
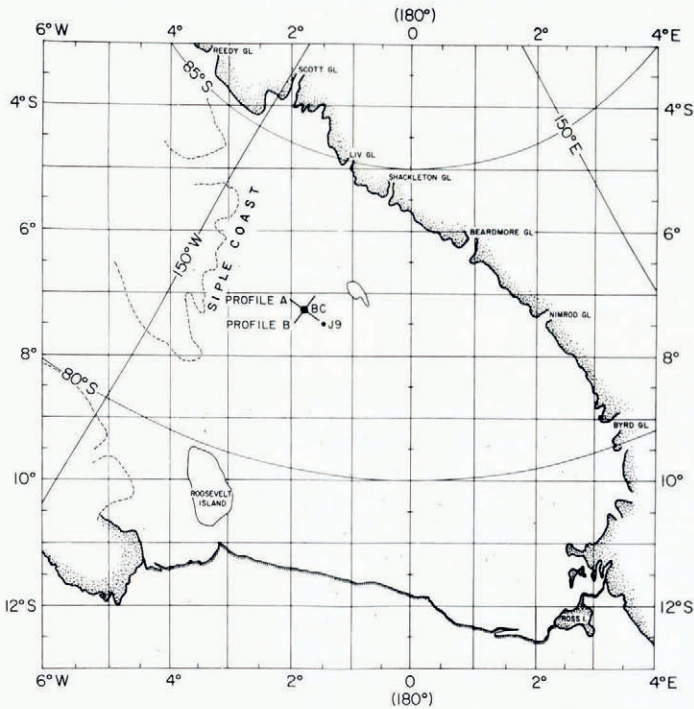

Fig. 1. Map of the Ross Ice Shelf showing the locations of stations BC and J9 and the orientations of the resistivity profiles. The rectangular network carries grid coordinates; circular arcs and radiating lines are geographic coordinates. The light dashed line marks the approximate grounding line between the ice shelf and the West Antarctic ice sheet. Gaps in the grounding line indicate probable ice streams.
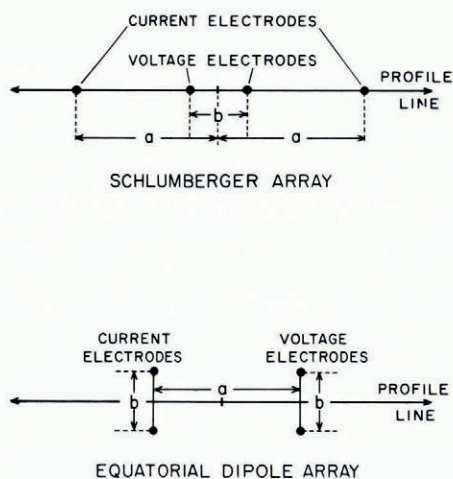
Fig. 2. Diagrams of the two types of array used in the resistivity measurements.

Both ground voltage and current were usually observed to decrease after the current circuit was closed, often by as much as an order of magnitude over a period of about 10 s. However, the ratio of voltage to current showed no consistent change with time, suggesting that polarization and induction effects were not seriously affecting the apparent resistivity values.

The principal difficulty in making resistivity measurements in such. a highly resistive medium as the ice is to maintain an adequate signal-to-noise ratio; noise levels must be minimized. Man-made electromagnetic signals from any kind of local radio broadcast (communications system, aircraft beacons, etc.) interfered seriously with the measurements and had to be stopped. The effect of natural micropulsations was highly variable. About one-third of the time the micropulsation level was negligible, about one-third of the time it caused noticeable drift of the zero point in the measurements, and about one-third of the time it was bad enough that measurements could not be made at all.

DATA REDUCTION

The basic data comprised sets of current I and voltage difference V measurements, each set consisting of several (usually six) series of simultaneous readings of I and V as they decayed, the direction of current flow being reversed for each new series. For each arrangement of the electrodes a plot of V versus I was drawn, defining (ideally) a straight line, the slope of which was taken as proportional to the apparent resistivity (e.g. Fig. 3a). (Using slopes rather than mean V/I ratios gives the heaviest weight to the strongest signals, which presumably represent the largest signal : noise ratios.) Not all sets satisfactorily defined single straight lines. In a few cases, owing either to a non-zero background voltage in the ice or to imperfect zeroing of the electrometer, there was a separation between points corresponding to opposite directions of current flow. In that case, the data were accepted if they could be satisfactorily fitted by two parallel straight lines with numerically equal V-intercepts of opposite sign (Fig. 3b; Fig. 3c shows an example of an unacceptable set). Where I varied too little to define satis-factory regression lines (e.g. Fig. 3f), means of the V/I ratios were accepted measures of the apparent resistivities.
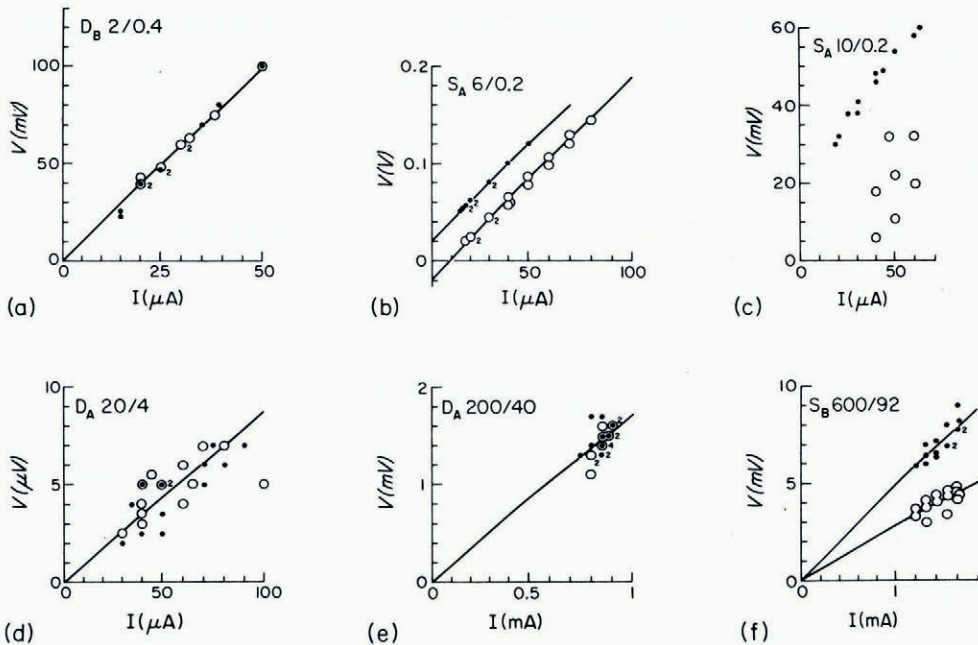
Fig. 3. Sample plots of potential difference (V) versus current (I). The individual measurements are identified by S for Schlumberger array, D for dipole array, subscripts A and B denoting the profile direction, and two numbers in the form a/b indicating the separations a and b. Open and solid circles denote current flow in opposite directions; small numbers indicate the number of readings plotted at the same point on the graph. Note that the scales are not the same for each plot.

The scatter exhibited by the various sets differed considerably (e.g. Fig. 3a and 3d); sets were still accepted so long as a regression line was well defined, since even scattered data yield standard errors which are small on the compressed scale of an apparent resistivity plot (e.g. Fig. 4). As electrode separations increased, the current tended to decay more slowly, sometimes becoming nearly constant (Fig. 3e). At the largest separations the currents were typically of equal magnitude in opposite directions, but the voltages in the two directions were often decidedly different (Fig. 3f). The electric field strengths corresponding to the imbalances in measured voltage were in the range of a few tens to a hundred millivolts per kilometer, reasonable values for natural telluric potentials.
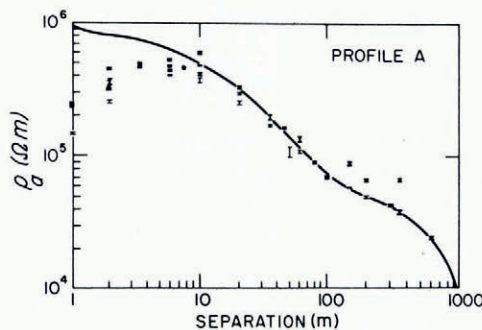

Fig. 4. Plot of all apparent resistivity data points, Profile A. Error bars show standard deviations from linear fits to plots like those in Figure 3. Heavier bars indicate a Schlumberger array, lighter bars a dipole array. The solid curve is calculated from Model 1 (see Table II).

Apparent resistivities[*], ρ_a, were calculated from the mean values of V/I according to the general formula

$$\rho_a = K \frac{V}{I},\tag{1}$$

wherein K has different values, K_s and K_d respectively, for the Schlumberger and dipole arrays.

The appropriate second-order K-factors for substitution in Equation (1) are

$$K_s = \frac{\pi a^2}{b}\left(1 - \frac{b^2}{4a^2}\right),$$

and

$$K_d = \frac{2\pi a^3}{b^2}\left(1 + \frac{3b^2}{4a^2}\right),$$

(Keller and Frischknecht, 1966; K_s is given by their equation (75), and K_d is readily derivable from their equation (72)). The spacings a and b have somewhat different meanings in the two cases (Fig. 2 and next paragraph).

In the numerical modeling described below, apparent resistivities have been calculated using the equation appropriate to the Schlumberger array

$$\rho_a = a^2 \left(\frac{\partial U}{\partial r}\right)_a,\tag{2}$$

where $(\partial U/\partial r)_a$ is the horizontal gradient of the normalized potential (see Appendix) at distance $r = a$ from a single electrode, and a is the separation (half-spacing) of the current electrodes (Fig. 2). Equation (2) is valid to the second order in a^2/b^2, where b is the potential-electrode separation (i.e. the length of the potential dipole). For the equatorial dipole array, the apparent resistivity is again proportional to the potential gradient, but a second-order correcting term is required:

$$\rho_a = a^2 \left(1 + \frac{3b^2}{8a^2}\right)\left(\frac{\partial U}{\partial r}\right)_a,\tag{3}$$

where b now represents the (identical) lengths of both the potential dipole and the current dipole, and a is the distance between their mid-points (Fig. 2). To avoid recalculating model apparent resistivities for the dipole array using Equation (3), thus requiring separate model fitting for the Schlumberger and dipole data, we have included the second-order factor from Equation (3) in the K factor, giving (to second order)

$$K_d' \equiv K_d \Big/ \left(1 + \frac{3b^2}{8a^2}\right) \approx \frac{2\pi a^3}{b^2}\left(1 + \frac{3b^2}{8a^2}\right).$$

When K_d' is used in place of K_d in Equation (1), the dipole data as well as the Schlumberger data can be compared directly to models calculated from Equation (2).

---

[*] The "apparent resistivity" is, by definition, the resistivity that a homogeneous half-space would have to have to yield the observed V/I ratio. More fundamentally, it can be thought of essentially as the gradient of the electrical potential arising from the injection of current into the earth, modified by a geometrical factor that compensates for the natural decrease in potential with increasing distance from the current source. The compensation for "geometrical spreading" makes the apparent resistivity more convenient to use for presentation of data and modeling results than the potential or the potential gradient, and it is the quantity generally used in electrical geophysics. The appellation itself is unfortunate, however, because it may seem to imply, erroneously, some simple relationship between the apparent resistivity at a particular electrode separation and the actual resistivity at a particular depth.

Apparent resistivities along Profiles A and B are shown in Figures 4 and 5; Schlumberger-array and dipole-array data along each profile have been plotted together. (The solid curves refer to a model discussed later.) A large scatter in observed values at the shorter distances is obvious; less obvious but still clear (especially in Figure 4) is a tendency for the dipole-array points to fall below the others at intermediate distances. Both of these characteristics can be explained if there are local inhomogeneities in the firn, such as ice lenses, wind crusts, or radiation crusts, that provide short conductive paths. These would naturally become more disturbing as the electrode separation was decreased, and, being local, would result in apparent resistivities that were not reproducible with electrodes in slightly different locations. It would follow further that the largest apparent resistivities at a particular separation probably best represent the bulk resistivity of the firn.
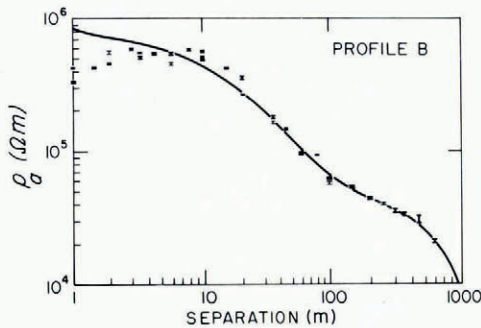

Fig. 5. Same as Figure 4, Profile B.

Assuming that near-surface inhomogeneities are indeed distorting the results, we have considered, for modeling purposes, only data for which the current-electrode spacing was greater than a certain minimum. That minimum was chosen, on the basis of consistency of the data, to be 10 m for Profile A and 8 m for Profile B. Thus, all measurements at plotted separations less than the minimum and, in addition, dipole measurements at separations less than 100 m on Profile A and 60 m on Profile B, were excluded from succeeding figures (except Figure 16 in the discussion of anisotropy). (Another reason not to use data at separations less than 8 or 10 m is that they are affected by seasonal warming in the upper few meters of the firn, which causes the observed decrease in ρ_a toward very small separations. Analysis of those data, which should yield information about the activation energy in the firn, will be carried out separately.) Right at 10 m on Profile A, only the higher of two points that differed by 50% was retained.

Three Schlumberger-array points on Profile A at relatively large separations (150 m, 200 m, and 350 m) were rejected simply because they showed discordantly high apparent resistivities compared with the rest of the data (Fig. 4), despite perfectly satisfactory V versus I plots. We have no specific explanation to offer for these discrepancies, but all three had much shorter voltage-electrode spacings than other, apparently satisfactory measurements at the same separation, suggesting that signal levels were below some instrumental noise level. No such problem arose with the Schlumberger-array measurements on Profile B or with dipole-array measurements on either profile. The selected points are listed in Table I and shown in Figures 6 and 7.

Three characteristic zones can be seen in the apparent resistivity data (and models, discussed below) at distances greater than 10 m. First, from 10 m to 100 m, is a region of rapidly decreasing ρ_a, corresponding to the strong effect of the increasing density with depth

TABLE I. ACCEPTED VALUES OF APPARENT RESISTIVITY

Standard deviations quoted are from linear fits to plots of V against I such as those in Figure 3.

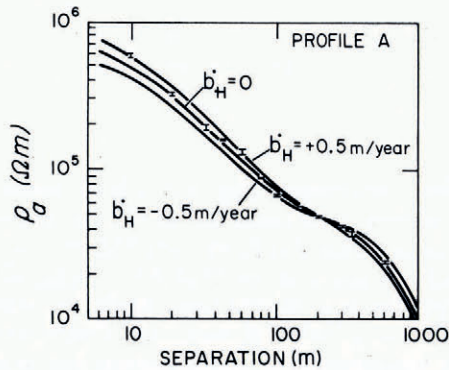| a m	Profile A Schlumberger array ρ_a Ω m	Profile A Dipole array ρ_a Ω m	Profile B Schlumberger array ρ_a Ω m	Profile B Dipole array ρ_a Ω m
8			6.4 ±0.1	
10	6.4 ±0.2		{6.3 ±0.1 / 5.7 ±0.1	
15			4.7 ±0.1	
20	3.7 ±0.1		4.0 ±0.1	
35	2.2 ±0.1		2.0 ±0.1	
45	1.81 ±0.01		1.60 ±0.04	
60	1.5 ±0.1		1.07 ±0.01	1.05 ±0.01
80	1.00 ±0.01		1.04	
100	0.780 ±0.004	0.76 ±0.01	0.69 ±0.01	0.64 ±0.02
150	0.644 ±0.001		0.59 ±0.01	
200		0.55 ±0.01	0.49 ±0.01	
250				0.44 ±0.01
300	0.47 ±0.01		0.39 ±0.01	
350	0.42 ±0.02		0.37 ±0.01	
450			0.34 ±0.02	
600	0.27 ±0.07		0.23 ±0.01	

Fig. 6. Selected data, Profile A, together with models showing the effect of changing b_H (Models 1, 6 and 7).
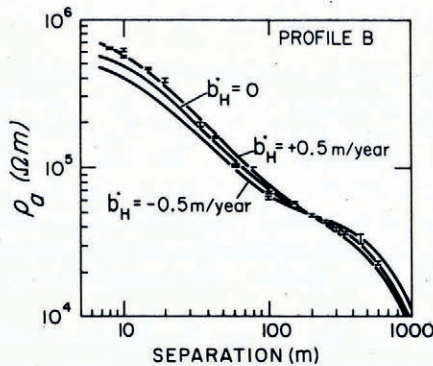

Fig. 7. Same as Figure 6, for Profile B.

in the upper 50 m of the ice shelf on the actual resistivity in the ice (Fig. 13). The effect of temperature in this zone is secondary, because the temperature change over this top 10% of the ice thickness is at most only a few degrees (Fig. 11). The marked decrease in slope at around 100 m is a direct result of the marked decrease in the density–depth gradient at the firn–ice boundary. In the next zone, from 100 m to about 500 m, the primary factor is the temperature gradient between depths of 50 m and 250 m in the ice. At distances greater than 500 m, in the third zone, apparent resistivities fall off increasingly more rapidly with distance owing to the increasingly important effect of the highly conductive sea-water beneath the ice shelf.

ANALYSIS

For the ease of computation, Hochstein (1967) fitted his apparent resistivity curve on the shelf ice with a sequence of layers of constant resistivity. A sequence of layers, however, does not well represent the real resistivity variation to be expected in an ice shelf. Because of the strong dependence of resistivity on density and temperature, and the continuous variation of each with depth, a model incorporating a continuous resistivity–depth function $\rho(z)$ is much to be preferred. We have therefore developed a computer program to calculate apparent resistivities on an ice shelf conforming to such a model. The relevant theory is laid out in the Appendix. The net result is a program which yields curves of apparent resistivity as a function of the vertical gradient $d(\ln \rho)/dz$ and the surface resistivity $\rho_0 \equiv \rho(0)$, the latter appearing only as a simple factor so that ρ_a/ρ_0 is independent of ρ_0. This means that changes of ρ_0 do not change the shape of any of the model curves of ρ_a or $\rho(z)$ shown in the figures of this paper, which all employ logarithmic scales, but merely raise or lower them.

The effect of temperature on the resistivity of solid ice is assumed to be in accordance with the Arrhenius function:

$$\rho \propto \exp (E/kT),$$

where E is the activation energy, k Boltzmann's constant (8.62×10^{-5} eV K^{-1} = 1.38×10^{-23} J K^{-1}), and T the absolute temperature. The corresponding term in $d(\ln \rho)/dz$ is $-(E/kT^2)(dT/dz)$. For specification of the temperature–depth function we employ the analysis of Crary (1961[a]) for a steady-state ice shelf of thickness H:

$$\frac{dT}{dz} = C \exp \left\{ \frac{1}{\alpha} \left[b_0 z - \frac{z^2}{2H} (b_0 + b_H) \right] \right\}, \tag{4}$$

where

$$C = \frac{T_H - T_0}{\displaystyle\int_0^H \exp \left\{ \frac{1}{\alpha} \left[b_0 z - \frac{z^2}{zH} (b_0 + b_H) \right] \right\} dz},$$

α is the thermal diffusivity, b the accumulation rate in thickness of ice, and the subscripts o and H refer to the surface and the base of the ice, respectively. (Equation (4) does not take into account the effect on advection of lower values of the density and diffusivity in the firn layers; inclusion would cause a modification of model ρ_a curves similar to that from doubling b_0, which is negligible for the purposes of this paper; see the DISCUSSION, below.)

The dependence of ρ on density is less well defined than its dependence on temperature. Following Glen and Paren (1975), we have tried two different equations that give the relative permittivity ϵ of a mixture of two different components of relative permittivities ϵ_1 and ϵ_2: Looyenga's equation (Looyenga, 1965)

$$\epsilon^{\frac{1}{3}} - \epsilon_1^{\frac{1}{3}} = v(\epsilon_2^{\frac{1}{3}} - \epsilon_1^{\frac{1}{3}}), \tag{5}$$

and Böttcher's equation (Böttcher, 1952)

$$\frac{\epsilon-\epsilon_I}{3\epsilon} = \frac{v(\epsilon_2-\epsilon_I)}{\epsilon_2+2\epsilon} . \tag{6}$$

In each, v is the volume proportion of the second dielectric. Both are based on the modification of solutions of Laplace's equation brought about by the introduction of small bodies of one permittivity into a medium of another permittivity. They differ in the permittivity contrast between the bodies and the surrounding medium; Looyenga's analysis appears better because of a differential approach that keeps the two permittivities always nearly equal during the gradual admixture. Glen and Paren point out the likelihood that these equations are at least mathematically valid for complex permittivities. We have extrapolated further to assume their applicability when the imaginary part of ϵ, $(\omega\epsilon_0\rho)^{-I}$, where ϵ_0 is the permittivity of free space, becomes very large with respect to the real part, i.e. when the frequency ω becomes very small. This leads, in the limit, to the case of d.c. conduction. Even though conduction currents replace displacement currents, Laplace's equation still holds in a grossly homogeneous medium if there is no free charge accumulation. In the firn layers, however, ρ is a strong function of z so $\nabla\cdot\mathbf{E}$ is not zero (see Appendix, Equation (A2)) and Laplace's equation is not valid. Looyenga's and Böttcher's equations thus do not lie on a firm physical foundation. Nevertheless, lacking a better theory, we try them on an empirical basis.

Equations (5) and (6), when applied to an air–ice mixture, reduce simply to

$$\rho_{firn} = \rho_{ice}/v^3,$$

for Looyenga's equation, and

$$\rho_{firn} = \frac{2\rho_{ice}}{3v-I},$$

for Böttcher's equation, where v is now the ratio of firn density to ice density. The corresponding contributions to $\dfrac{d(\ln \rho)}{dz}$ are $-\dfrac{3}{v}\dfrac{dv}{dz}$, and $-\dfrac{3}{3v-I}\dfrac{dv}{dz}$, respectively.

The effect of pressure on the resistivity of the solid ice is negligible in the ice shelf. At the base of an ice shelf 500 m thick the pressure is less than 50 bars (5 MN m^{-2}), corresponding to a resistivity change of less than 1% (Chan and others, 1965). However, Hochstein (1967) found that an empirical relationship based on pressure appeared to fit measured resistivities on firn cores fairly well down to the sampling depth limit of 15 m, and he suggested the extrapolation of that relationship to greater depth. We have, therefore, tried his model

$$\rho \propto p^{-0.35},$$

where p is the hydrostatic pressure, as a substitute for a direct density dependence. The corresponding contribution to $d(\ln \rho)/dz$ is $(-0.35/p)\ dp/dz$.

APPLICATION TO ROSS ICE SHELF MEASUREMENTS

To apply the analysis to the field measurements, the variation of density with depth is needed. Measurements at station BC extend only to a depth of 10 m; for greater depths in the firn, the density was calculated from the variation of seismic compressional-wave velocity with depth, using a velocity–density relationship developed by Kohnen (1972). The wave velocities were in turn determined from seismic refraction shooting along two profiles that coincided with the resistivity profiles. The velocity–depth functions that were found (Robertson, unpublished) were slightly different in the two directions, the velocities (and hence the calculated densities) being higher along Profile A for depths less than 50 m (Fig. 8). The velocity differences are large enough to be real, indicating some seismic anisotropy in the firn.
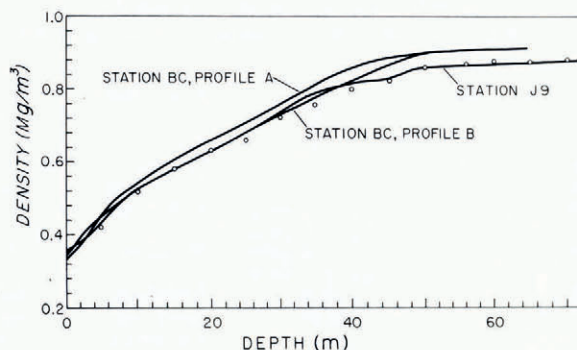
Fig. 8. Density–depth plots calculated from seismic refraction shooting (lines), and density measurements on ice cores from station J9 (circles).

We have adopted densities calculated along Profile B, because anisotropy is more likely to raise the velocity above the isotropic value than to lower it, and because Profile B yielded densities that were closer to actual density measurements (Langway, 1975; also shown in Fig. 8) in a hole drilled in November 1974 at station J9 (Fig. 1). Had densities been calculated from seismic velocities along Profile A rather than Profile B, model apparent resistivities would have been about 10% higher between roughly 30 and 100 m, the difference diminishing rapidly outside that range. Such a change would not significantly alter the model fits.

Use of Crary's equation (Equation (4)) for estimating the temperature distribution required numerical values for several parameters. The ice thickness H was taken to be 493 ± 10 m from radar soundings by J. W. Clough (Robertson, unpublished); we took the surface balance rate b_0 to be 0.08 m year^{-1} as determined by Clausen and Dansgaard (in press), from identification of radioactive fallout horizons; the basal temperature T_H was assumed to be $-2°$C, the freezing point of sea-water, and the thermal diffusivity α was taken to be 1.2×10^{-6} m^2 s^{-1} (Crary, 1961[a]). Of these quantities, the only one about which there is great enough uncertainty to be of possible significance is b_0; the values found throughout the region by Clausen and Dansgaard (in press) were only half as great as those determined from pit studies on I.G.Y. traverses (Crary and others, 1962). This uncertainty turns out to be of minor, if not completely negligible importance (see Discussion, below).

We treat the activation energy E and the basal balance rate b_H, as parameters to be varied in attempts to fit the observed apparent resistivity curve.

Model fitting

As an initial model, we chose $E = 0.25$ eV (24 kJ mol^{-1}) in accordance with measurements on ice-sheet ice from "Byrd" station and elsewhere (Fitzgerald and Paren, 1975; Glen and Paren, 1975), $b_H = 0$, and Looyenga's equation for the density effect (Model 1; for a list of all models considered in this paper see Table II). ρ_0 was varied to provide a best fit of the model to the observations at separations greater than 100 m corresponding to conduction principally in solid ice. The fit to both profiles at those separations is very good (middle of the three curves in Figs 6 and 7) showing that the chosen values of E and b_H are completely in accord with the data. The value of ρ_0, however, is 12% higher for Profile A than for Profile B. Since changes in ρ_0 do not change the shape of the ρ_a curves, we may combine the results of Profile B with those of Profile A simply by shifting them uniformly upward by 12% (Figs 10, 12, 14, and 15) for study of the average characteristics of the ice. We will consider later the question of the apparent anisotropy.

TABLE II. APPARENT RESISTIVITY MODELS

The figure numbers quoted in the last three columns indicate where plots resulting from the models can be found.

Model No.	b_0 m year^{-1}	b_H m year^{-1}	E eV	Density model	Figure No. ρ_a	$T(z)$	$\rho(z)$
1	0.08	0	0.25	Looyenga	4–7, 10, 14	11	9, 13
2	0.08	0	0.25	Böttcher	10		9
3	0.08	0	0.25	Hochstein	10		9
4	0.08	0	1, $z < 40$ m 0.25, $z > 40$ m	Looyenga	12		
5	0.08	0	1, $z < 40$ m 0.25, $z > 40$ m	Böttcher	12		
6	0.08	+0.5	0.25	Looyenga	6, 7	11	13
7	0.08	−0.5	0.25	Looyenga	6, 7	11	13
8	0.08	0	0.4	Looyenga	14		13
9	0.16	0	0.25	Looyenga	14		
10	0.08	+0.5	0.15	Looyenga	15		
11	0.08	−0.5	0.4	Looyenga	15		

At separations less than 100 m the model curves reflect principally the effect of density variations. The fit to Profile A appears satisfactory, but that to Profile B and to the combined profiles is not so good, particularly if it is true that the higher apparent resistivities at a particular distance are to be preferred.

Choice of model of density dependence

We next tried Böttcher's equation for $\rho(v)$ and Hochstein's equation for $\rho(p)$ (Models 2 and 3; Figs 9 and 10). Model 3 is entirely wrong in shape, with too small a resistivity gradient above 50 m and too large a gradient below. Clearly, the resistivity is a function of density, as expected, rather than of pressure. Hochstein's relation has therefore not been considered further.

Model 2, matched to Model 1 at distances greater than 200 m, has the right shape but insufficient range in ρ_a. The reason is that $d(\ln \rho)/dz$ is steeper for Model 1 in the critical depth range of 20–100 m. It appears that Looyenga's equation fits significantly better than Böttcher's. Even a large bottom-freeze rate ($b_H > 0$), which would greatly increase the temperature gradient in the upper part of the shelf (e.g. $b_H = +0.5$ m year^{-1}, Fig. 11), would not increase ρ_a enough at small separations (cf. curves for $b_H = 0$ m year^{-1} and $b_H = 0.5$ m year^{-1} in Figs 6 or 7) to bring Model 2 into agreement with the observed apparent resistivities.
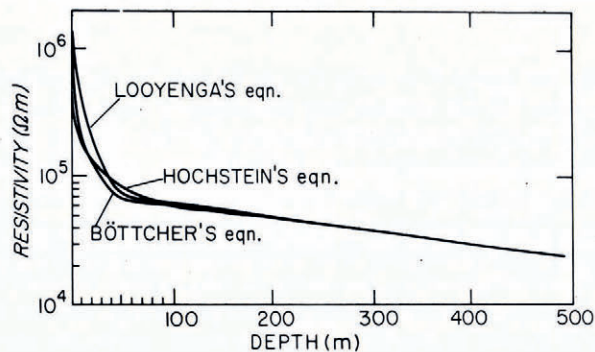

Fig. 9. *Resistivity versus depth in the ice shelf according to three different models of resistivity as a function of density (Models 1, 2 and 3).*
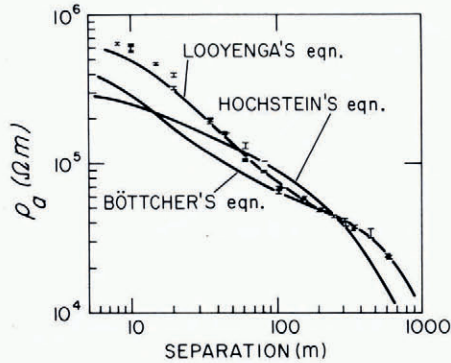
Fig. 10. Apparent resistivity curves following from the three models in Figure 9, compared with combined data from Profiles A and B.
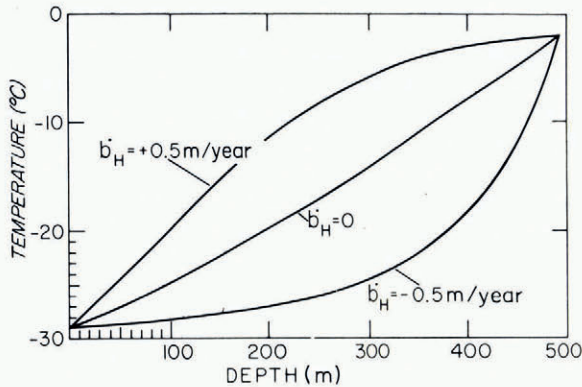

Fig. 11. Calculated temperatures versus depth assuming $b_0 = 0.08$ m/year and b_H as indicated (Models 1, 6 and 7).

One other factor must be considered, however. The activation energy appropriate to the firn is probably much higher than that for ice. Kopp (1962) found values of 0.7 eV (67 kJ mol⁻¹) for compressed fresh snow, around 0.9 eV (87 kJ mol⁻¹) for compressed granular snow and from 0.8 eV (77 kJ mol⁻¹) to as high as 1.4 eV (135 kJ mol⁻¹) for samples from depths of 10 to 40 m in the Greenland ice sheet; his observations for compressed snow have recently been confirmed by Fitzgerald and others (in press). Kopp associates the high activation energies with conduction in the quasi-fluid film which exists on the outer surface of the ice grains. To take this factor into account, we have tried a simple model in which the activation energy is taken to be 1.0 eV (96 kJ mol⁻¹), corresponding to grain-surface conduction, down to the firn–ice boundary at a depth of 40 m, and 0.25 eV (24 kJ mol⁻¹), corresponding to bulk conduction, at greater depth. The result (Fig. 12) is an increased slope in the calculated apparent resistivities at separations less than 100 m that brings the "Looyenga model" (Model 4) into remarkably close agreement with the observations, while still leaving the "Böttcher model" (Model 5) substantially too low. Only if there is a temperature gradient in the upper 50 m of the ice large even in comparison with that calculated for a 0.5 m year⁻¹ bottom accumulation rate, could the "Böttcher model" be brought into agreement with the observations. Further consideration of this problem will have to await resistivity measurements at a drill-hole site where the temperature variation with depth is known.
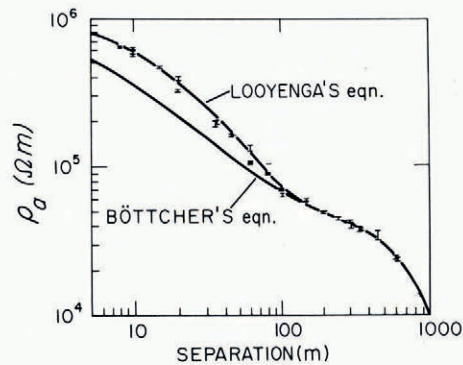
Fig. 12. *Apparent resistivity curves for Models 4 and 5, showing the effect of taking $\epsilon = 1.0\,eV$ ($96\,kJ\,mol^{-1}$) near the surface. Data are combined from Profiles A and B.*

Despite the good agreement with the observations, it should be borne in mind that the adoption of Looyenga's relation for d.c. conduction in the firn layers does not rest on a firm physical foundation, particularly if conduction along grain surfaces is indeed the dominant mechanism, and that close agreement, therefore, is not necessarily to be expected. Thus in examining the effects of changing various parameters, care must be taken not to be influenced by the goodness of fit between models and observations at distances less than 100 m. Partly to emphasize that fact, the remaining modeling in this paper is done on the basis of values of E that are constant throughout the thickness of the ice shelf.

Changes of $\dot{b}_H$, E, and $\dot{b}_0$

The rather large values $\dot{b}_H = \pm 0.5$ m year^{-1} (Models 6 and 7) yield the temperature profiles, $\rho(z)$ functions, and apparent resistivity curves shown, together with corresponding curves for $\dot{b}_H = 0$, in Figures 11, 13, 6, and 7. The three apparent resistivity curves have been matched, arbitrarily, at a distance of 200 m, which also has the effect of providing about the best fit for each curve. Although the differences between models are slight, the curve for $\dot{b}_H = 0$ does appear to fit both profiles (Figs 6 and 7) significantly better than those for rapid rates of bottom freeze or bottom melt. If other assumptions are correct, the resistivity measurements thus indicate that the bottom balance rate is numerically less than 0.5 m year^{-1}.
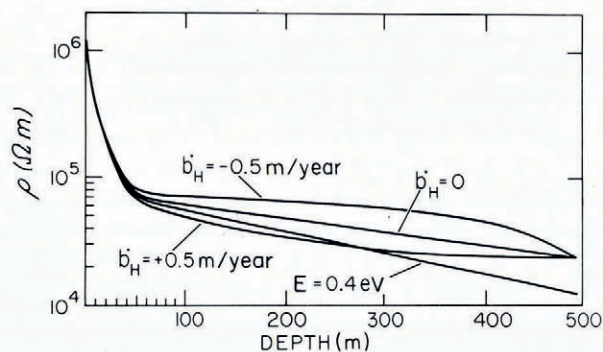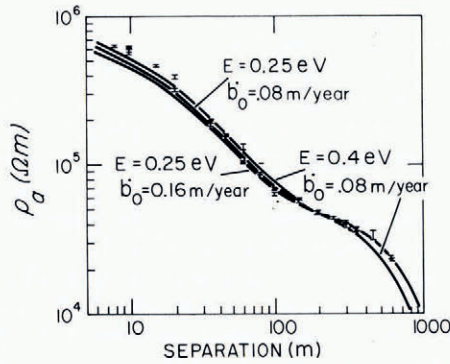

Fig. 13. *Resistivity versus depth for Models 1, 6, 7 and 8.*

Fig. 14. Models of apparent resistivity showing the effects of changing ε and b_0 (Models 8 and 9). Data are combined from Profiles A and B.

Hochstein's (1967) analysis of resistivities near Roosevelt Island led to an estimate of E between 0.3 and 0.5 eV (29–48 kJ mol⁻¹); we have tried $E = 0.4$ eV (38 kJ mol⁻¹) (Model 8) with the results shown in Figures 13 and 14. Model curves are again matched at 200 m. The fit for $E = 0.25$ eV (24 kJ mol⁻¹) is clearly superior to that for $E = 0.4$ eV (38 kJ mol⁻¹) if the bottom balance rate is small.

Because of the discrepant estimates of surface balance rates mentioned above, an apparent resistivity curve has been calculated for a model in which b_0 has been doubled, to 0.16 m/year (Model 9). The change in the calculated resistivities (Fig. 14) is imperceptible at distances greater than 200 m, and trivial at all distances.

Since E and b_H are both related to the temperature effect on the resistivity, one might expect to be able to vary both of them in such a way as to maintain a fit to the data. This is indeed the case, as seen from Models 10 and 11 (Fig. 15). The decreased temperature gradient in the upper half of the shelf that results from increasing the bottom melt rate can be compensated for by increasing the activation energy; conversely, the effect of bottom freezing with the attendant increase in the upper temperature gradient can be balanced by a smaller activation energy. In the light of other evidence, however, the most likely combination is E close to 0.25 and b_H close to 0.
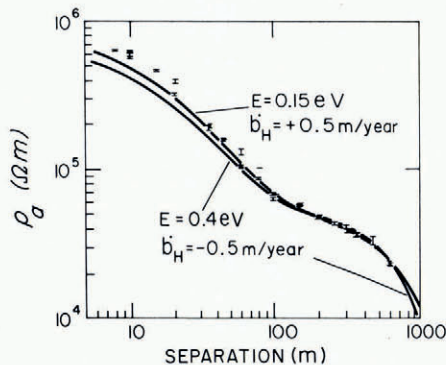

Fig. 15. Models of apparent resistivity showing simultaneous changes in ε and b_H (Models 10 and 11).

ABSOLUTE RESISTIVITY

Up to this point we have been discussing the shape of the apparent resistivity curves, i.e. resistivity ratios relative to an unspecified ρ_0. We now wish to consider the actual magnitude of the resistivity in the solid ice. There is no simple correspondence between a measured apparent resistivity and the actual resistivity at any particular depth—ρ_a at a particular distance depends on ρ over a whole range of depths. Thus to estimate ρ at a particular depth we must assume a specific model. (Note that the model chosen need not correspond to the correct melt/freeze rate or activation energy; it need only yield the correct resistivities.)

The best fit to the observations comes from Model 4 (Fig. 12), which indicates an actual resistivity at a depth of 100 m of 7.4×10^4 Ω m according to Profile A, and 6.6×10^4 Ω m according to Profile B. (100 m was chosen for the depth simply as a round value within the range where the actual resistivities strongly affect the apparent resistivity at the separation (200 m) at which models and observations were matched.) We can get an idea of the uncertainty in the resistivity by considering Models 1, 10, and 11 (Figs 6 or 7 and 15), which yield apparent resistivity curves very similar to each other but falling significantly below Model 4. The resistivities at 100 m according to these models lie within $\pm 1\%$ of 6.3×10^4 Ω m (for Profile A), 15% less than the estimate from Model 4. In view of the substantially better fit of Model 4 to the observed data, the author believes that the corresponding average resistivity, 7×10^4 Ω m, should be in error by less than 10%.

The temperature at 100 m depth, assuming steady-state with $b_H = 0$, is $-23°C$. The corresponding average conductivity, 1.4×10^{-5} Ω^{-1} m^{-1}, is just about twice the values found by Hochstein (1967) from his resistivity profiles on Roosevelt Island and immediately adjacent on the Ross Ice Shelf, and by Fitzgerald and Paren (1975) from laboratory measurements on samples from the deep core at "Byrd" station, although well within the range of other measurements from cold, polar glaciers and ice sheets (Glen and Paren, 1975).

The accuracy of the resistivity measurements on Antarctic ice both in the field and in the laboratory is certainly great enough that a factor of two must have physical significance, i.e. that the ice at station BC is truly about twice as conductive as the ice at "Byrd" station to the east and the ice on and near Roosevelt Island to the north. There is no reason to suppose that the snow from which the ice at station BC formed was inherently more conductive than that around Roosevelt Island or "Byrd" station (since the ice at 100 m depth is about 1 000 years old, it presumably fell on the surface near the Siple Coast grounding line about 200 km upstream). Indeed, one might instead expect ionic impurities derived from the Ross Sea (Langway and others, 1974) in the snow at Roosevelt Island to increase conductivities there, but there is no evidence of such an effect. The conductivity difference therefore probably reflects some difference in the densification or strain history of the ice in the different locations. Although it is difficult to say just what the significant difference in history might be until the basic cause for the remarkably high conductivity of polar ice in general is better known, resistivity profiles might nevertheless be useful in tracing flow lines in ice shelves, where movement rates are great enough that ice at a few hundred meters depth originated a significant distance up-stream.

The difference in the apparent resistivities along the two perpendicular profiles is also presumably a real physical phenomenon, but its significance is not clear. When the apparent resistivities from Profiles A and B are plotted together as measured (Fig. 16), rather than with an adjustment to match at a separation of 200 m, no consistent difference at separations less than 30 m appears, whereas an apparent anisotropy seems to be fully developed at distances greater than that. At a separation of 30 m the current flows almost entirely above the firn/ice boundary, so it is unlikely that any true crystalline anisotropy associated with a strongly developed preferred orientation of c-axes is responsible. It is probably significant in this regard that the field measurements at 30 m on Profile B were sufficiently disturbed to
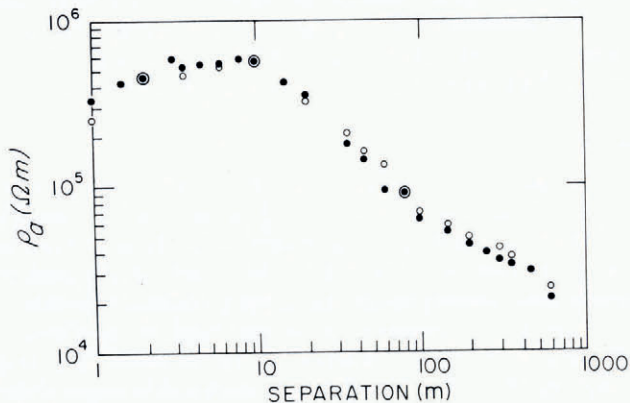
Fig. 16. Apparent resistivity data points as measured on the two profiles, without adjustment for anisotropy. The highest value at each separation from each profile has been plotted. Profile A: open circles; Profile B: solid circles.

preclude any valid determination of the apparent resistivity (according to the criteria given above), and that the measurements at 35 m were still not of the highest quality. (No such difficulty was observed at 35 m on Profile A; unfortunately, measurement was not made at 30 m.) This suggests that there is some kind of conductivity anomaly at a depth of a few tens of meters or less—perhaps a healed crevasse. (The nearest present-day crevasses in a generally up-stream direction are about 70 km (300 years) away, corresponding to a depth of burial of about 40 m.)

Discussion

Resolution of temperatures and basal melt/freeze rate

Model fitting led to the conclusion that the bottom balance rate lies between +0.5 m year^{-1} and −0.5 m year^{-1}—the uncertainty is too large for the result to have much glaciological significance. However, the resolving power of the apparent resistivity models with respect to dT/dz and hence to $\dot{b}_H$ would be greatly improved if the models could be matched at 10 m, or even 100 m, instead of 200 m. This should be possible when resistivity measurements are completed at a site of known $T(z)$, so that the value of the activation energy can be confirmed and the relationship between resistivity and density better determined. (Such measurements are planned for the RISP drill site in 1976–77.) Thereafter, it may be possible in other localities to determine T in the upper half of the ice shelf to within a degree or two, and thus estimate $\dot{b}_H$ with a resolution of perhaps ±0.1 m year^{-1}; both are capabilities that would be of distinct glaciological value.

For two reasons, however, there is no part of the apparent resistivity curve that reflects at all sensitively the temperature gradient in the lower part of the shelf. In the first place, resistivities in that part of the shelf are largely masked by the effect of the sea-water, and in the second, the rapid decrease in apparent resistivity with distance causes a rapid decrease in potential difference between measuring electrodes as their separation is increased thus lowering the signal into the noise level. Even if the range of measurements could be increased by some means of enhancing the signal : noise ratio, the first problem remains; it seems unlikely, therefore, that resistivity profiles can ever be used to examine directly the temperature variations in the lower half of an ice shelf. Only a major change in the resistivity of the ice, either upward or downward, might be detectable. An order-of-magnitude decrease near the bottom, such as could result from the freeze-on of saline ice, might be detected, whereas

a large increase in the resistivity at the base of the shelf, even in a layer only ten or a few tens of meters thick should be readily detectable. (An increase in apparent resistivity at distances greater than 600 m does indeed appear on preliminary results of a resistivity profile south of Roosevelt Island, but the data have not yet been analyzed in detail.)

Steady-state assumption

The assumption was made in the analysis that the ice shelf is in steady-state. If it is not, and there is good reason to believe it may not be (Thomas, 1976), then Crary's equation for the englacial temperatures (Equation (4)) is no longer valid. In that case, analysis of apparent resistivity curves by the procedure we have outlined here can still proceed, leading to a steady-state temperature profile that approximates the actual, transient profile. Alternatively, the calculation of temperatures in our computer program could be modified in accordance with any specific model of transient dynamic behavior of the ice shelf. The resistivity data could thus be very useful in distinguishing between dynamic models that imply different temperature–depth curves, particularly if the bottom balance rate were known independently from ice-thickness, movement rate, and surface-strain measurements.

REFERENCES

Böttcher, C. J. F. 1952. *Theory of electric polarization.* Amsterdam, Elsevier.
Chan, R. K., *and others.* 1965. Effect of pressure on the dielectric properties of ice I, [by] R. K. Chan, D. W. Davidson and E. Whalley. *Journal of Chemical Physics,* Vol. 43, No. 7, p. 2376–83.
Clausen, H. B., *and* Dansgaard, W. In press. Less surface accumulation on the Ross Ice Shelf than hitherto assumed. [Paper presented at International Symposium on Isotopes and Impurities in Snow and Ice, Grenoble, 1975.]
Crary, A. P. 1961[a]. Glaciological regime at Little America station, Antarctica. *Journal of Geophysical Research,* Vol. 66, No. 3, p. 871–78.
Crary, A. P. 1961[b]. Glaciological studies at Little America station, Antarctica, 1957 and 1958. *IGY Glaciological Report Series* (New York), No. 5.
Crary, A. P., *and others.* 1962. Glaciological regime of the Ross Ice Shelf, by A. P. Crary, E. S. Robinson, H. F. Bennett and W. W. Boyd, Jr. *Journal of Geophysical Research,* Vol. 67, No. 7, p. 2791–807.
Fitzgerald, W. J., *and* Paren, J. G. 1975. The dielectric properties of Antarctic ice. *Journal of Glaciology,* Vol. 15, No. 73, p. 39–48.
Fitzgerald, W. J., *and others.* In press. Are the anomalous dielectric properties of polar ice due to impurities? By W. J. Fitzgerald, J. W. Glen and J. G. Paren. [Paper presented at International Symposium on Isotopes and Impurities in Snow and Ice, Grenoble, 1975.]
Glen, J. W., *and* Paren, J. G. 1975. The electrical properties of snow and ice. *Journal of Glaciology,* Vol. 15, No. 73, p. 15–38.
Hochstein, M. P. 1967. Electrical resistivity measurements on ice sheets. *Journal of Glaciology,* Vol. 6, No. 47, p. 623–33.
Hochstein, M. P., *and* Risk, G. F. 1967. Geophysical measurements on the McMurdo Ice Shelf, Antarctica during 1965–66. *New Zealand. Dept. of Scientific and Industrial Research. Geophysics Division, Report* No. 47.
Keller, G. V., *and* Frischknecht, F. C. 1966. *Electrical methods in geophysical prospecting.* Oxford, etc., Pergamon Press. (International Series of Monographs on Electromagnetic Waves, Vol. 10.)
Kohnen, H. 1972. Über die Beziehung zwischen seismischen Geschwindigkeiten und der Dichte in Firn und Eis. *Zeitschrift für Geophysik,* Bd. 38, Ht. 5, p. 925–35.

Kopp, M. 1962. Conductivité électrique de la neige, au courant continu. *Zeitschrift für angewandte Mathematik und Physik*, Vol. 13, Fasc. 5, p. 431–41.
Langway, C. C., jr. 1975. Antarctic ice core studies. *Antarctic Journal of the United States*, Vol. 10, No. 4, p. 152–53.
Langway, C. C., jr., *and others*. 1974. Chemical profile of the Ross Ice Shelf at Little America V, Antarctica, by C. C. Langway, Jr., M. Herron and J. H. Cragin. *Journal of Glaciology*, Vol. 13, No. 69, p. 431–35.
Looyenga, H. 1965. Dielectric constants of heterogeneous mixtures. *Physica*, Deel 31, No. 3, p. 401–06.
Robertson, J. D. Unpublished. Geophysical studies on the Ross Ice Shelf, Antarctica. [Ph.D. thesis, University of Wisconsin–Madison, 1975.]
Sunde, E. D. 1949. *Earth conduction effects in transmission systems*. New York, Dover Publications, Inc.
Thomas, R. H. 1976. Thickening of the Ross Ice Shelf and equilibrium state of the west Antarctic ice sheet. *Nature*, Vol. 259, No. 5540, p. 180–83.

APPENDIX

THEORY OF APPARENT RESISTIVITY

The differential equation governing the electrical potential from a single, d.c., point source of current in a conducting medium may be very simply developed. Ohm's law gives

$$\mathbf{E} = \rho(x, y, z)\,\mathbf{j},$$ (A1)

where $\mathbf{E}$ is the electric field, ρ is the electrical resistivity (in general a function of all coordinates) and $\mathbf{j}$ is the current density. Conservation of electric charge requires, for steady state

$$\nabla \cdot \mathbf{j} = 0,$$

whence, from Equation (A1)

$$\nabla \cdot \mathbf{E} - \frac{1}{\rho}\,\nabla \rho \cdot \mathbf{E} = 0.$$ (A2)

Let the electrical potential u be defined by

$$\mathbf{E} = \nabla u,$$ (A3)

then Equation (A2) becomes

$$\nabla^2 u - \frac{1}{\rho}\,\nabla \rho \cdot \nabla u = 0,$$

which can be rewritten

$$\nabla^2 u - \nabla(\ln \rho) \cdot \nabla u = 0.$$ (A4)

For application to an ice shelf, we assume that ρ varies only with depth z. We also adopt cylindrical coordinates, appropriate to the point source. Since we are interested in voltage : current ratios, it is convenient to define a normalized potential $U = 2\pi u/I$, where I is the input current. By symmetry, U will be a function of z and the radial distance r only. Then, from Equation (A4)

$$\frac{1}{r}\frac{\partial}{\partial r}\left(r\frac{\partial U}{\partial r}\right) + \frac{\partial^2 U}{\partial z^2} - \frac{d(\ln \rho)}{dz}\frac{\partial U}{\partial z} = 0.$$ (A5)

Next, consider the boundary conditions appropriate to the ice shelf. The geometrical arrangement is shown as (a) in Figure A1; the requirements are that there be no vertical component of current at the surface, whence $\partial U/\partial z = 0$ at $z = 0$; that the potential and its normal derivative be continuous at $z = H$; that (by symmetry) $\partial U/\partial r = 0$ at $r = 0$, $z \neq 0$; and that $U \to 0$ as $r \to \infty$.
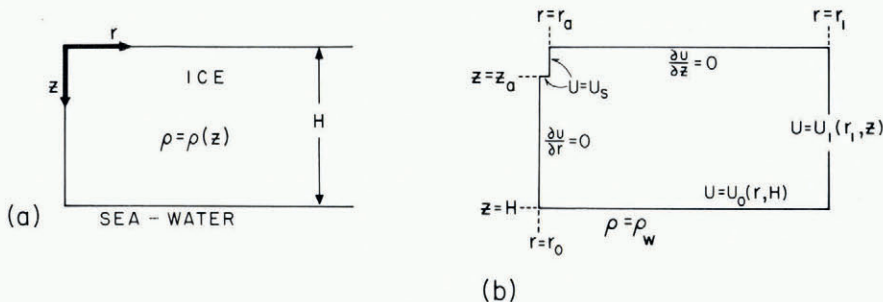

Fig. A1. *Diagram of the coordinate system and boundary values for the solution of the electrical potential equation.*

The solution, call it U_i, in the simple case of constant resistivity ρ_i in the ice and ρ_w in the water is well known (e.g. Sunde, 1949, section 2.5):

$$U_i(r, z) = \rho_i \left[\frac{1}{(z^2+r^2)^{\frac{1}{2}}} - \int_0^\infty \frac{\mu_i \exp{(-2\lambda H)}}{1 + \mu_i \exp{(-2\lambda H)}} \left[\exp{(\lambda z)} + \exp{(-\lambda z)} \right] \mathcal{J}_0(\lambda r)\, d\lambda \right], \qquad (A6)$$

where $\mathcal{J}_0$ is the zero-order Bessel function, and $\mu_i = (\rho_i - \rho_w)/(\rho_i + \rho_w)$.

When ρ varies arbitrarily with z, an explicit solution cannot be written; some sort of approximate solution must then be sought for any particular $\rho(z)$. The usual approach is to approximate $\rho(z)$ by a series of layers, or by some simple function for which an explicit solution can be found. The approach taken here is different—to find a numerical solution to the differential equation (A5) with the exact $\rho(z)$ desired.

For numerical analysis, two of the boundary conditions must be expressed differently. Since we have no analytical solution to Equation (A5), we know neither the potential nor its normal derivative at $z = H$. Fortunately, the resistivity of sea-water ($\approx \frac{1}{3}\ \Omega\ m$) is orders of magnitude less than that of glacier ice ($> 10^4\ \Omega\ m$), so that U is very small at $z = H$. For analytical purposes it would suffice to take $\rho_w = 0$, hence $U = 0$, at $z = H$, but this is not convenient numerically. Instead we assume that $U(r, H) = [U_i(r, H)]_{\rho_i = \rho_0} \equiv U_0(r, H)$, i.e. that U differs insignificantly from the very small value it would have in a shelf with constant resistivity equal to the actual resistivity ρ_0 at $z = 0$. (The *proportional* difference between $U_0(r, H)$ and $U(r, H)$ may be large, but that does not matter since both are very small compared to $U(r, 0)$.) To find $U_0(r, H)$ in a form useful for numerical calculations, expand the term $[1 + \mu_i \exp{(-2\lambda H)}]^{-1}$ in Equation (A6) and use the identity

$$\frac{1}{(r^2+w^2)^{\frac{1}{2}}} = \int_0^\infty \exp{(-\lambda w)}\, \mathcal{J}_0(\lambda r)\, d\lambda,$$

to obtain

$$U_i(r, z) = \rho_i \left[\frac{1}{(z^2+w^2)^{\frac{1}{2}}} + \sum_{n=1}^\infty (-1)^n \mu_i{}^n \{ [(2nH + z)^2 + r^2]^{-\frac{1}{2}} + [(2nH - z)^2 + r^2]^{-\frac{1}{2}} \} \right] \qquad (A7)$$

Then

$$U_0(r, H) = \rho_0 \left\{ (1 - \mu_0) \sum_{n=0}^\infty (-1)^n \mu_0{}^n [(2n+1)^2 H^2 + r^2]^{-\frac{1}{2}} \right\}, \qquad (A8)$$

wherein $\mu_0 \equiv [\mu_i]_{\rho_i = \rho_0}$.

A similar situation obtains for large values of r. Since we cannot apply a numerical condition at $r = \infty$, we take instead as the boundary $r = r_1$, where $r_1 \gg H$ so that the effect of the shelf is small. Again, setting $U = 0$ is numerically inconvenient; we choose instead an approximation to the real potential distribution which can be used not only as a boundary condition at $r = r_1$, but also as an initial value for the numerical iterations at all points.

The assumption is that the electric field at any point can be approximated by the field that would exist in the ice if the resistivity throughout were equal to its actual value at that point. Then for the corresponding potential, call it U_1, we have, from Equation (A3),

$$\nabla U_1 = [\nabla U_i]_{\rho_i = \rho(z)}. \qquad (A9)$$

To build up a U_1 field in the ice shelf, we start with the approximation (8) and integrate upwards:

$$U_1 = U_0(r, H) + \int_H^z \frac{dU_1(r_1 z)}{dz}\, dz. \qquad (A10)$$

Since the series in Equation (A7) is alternating with diminishing terms, it converges uniformly and can be differentiated term by term, whence, using Equation (A9),

$$\frac{\partial U_1}{\partial z} = \rho(z) \left[\frac{-z}{(z^2+r^2)^{3/2}} + \sum_{n=1}^\infty (-1)^n \mu^n(z) \left\{ \frac{2nH - z}{[(2nH - z)^2 + r^2]^{3/2}} - \frac{2nH + z}{[(2nH + z)^2 + r^2]^{3/2}} \right\} \right] \qquad (A11)$$

The boundary condition at $r = r_1$ is simply $U(r_1, z) = U_1(r_1, z)$.

The final step in comparing theory with measurements is to calculate the apparent resistivity ρ_a. For a Schlumberger array, in which the distance between potential electrodes is small compared to that between current electrodes,

$$\rho_a = a^2 \left[\frac{\partial U}{\partial r} \right]_{r = a,\ z = 0}, \qquad (A12)$$

where a is the mean distance from potential to current electrodes (Fig. 2).

For numerical calculations we must consider the source as having finite size; we define the potential on a small rectangular notch of dimensions r_a and z_a. The simplest source potential is that, call it U_s, for a semi-infinite medium of resistivity ρ_0:

$$U_s(r, z) = \frac{\rho_0}{(z^2 + r^2)^{\frac{1}{2}}} \; ;$$

we therefore specify $U = U_s(r, z)$ along $r = r_a$, $0 \leqslant z \leqslant z_a$, and $z = z_a$, $0 \leqslant r \leqslant r_a$.

The boundary conditions, including the source function, may be summarized (Fig. A1b):

(a) on $z = z_a$, $r \leqslant r_a$, $\quad U = U_s(r, z_a)$;

(b) on $z = 0$, $\quad r > r_a$, $\quad \dfrac{\partial U}{\partial z} = 0$;

(c) on $z = H$, $\quad\quad\quad U = U_0(r, H)$;
(d) on $r = r_a$, $z \leqslant z_a$, $\quad U = U_s(r_a, z)$;

(e) on $r = 0$, $\quad z > z_a$, $\quad \dfrac{\partial U}{\partial r} = 0$;

(f) on $r = r_1$, $\quad\quad\quad U = U_1(r_1, z)$.

The problem is now well posed, and solutions may be obtained by finite differences, subject to the specification of $d(\ln \rho)/dz$. For applying finite differences with a constant grid size, changes of independent variables are convenient; let $g = \ln r$ (r in meters) and $y = z^{2/3}$. The first provides the logarithmic horizontal scale standard in resistivity work, while at the same time allowing the grid spacing in r to increase appropriately with distance. The second provides a much more limited scale expansion—since the temperature, and hence ρ, may be expected to change rapidly with depth in the lower part of the shelf, too great a scale modification (such as a logarithmic scale) would be inadvisable. The transformation chosen yields grid point intervals in z of one or two meters near the surface, and about 10 m at the base of the ice.

Boundary condition (e) must now be modified since $g \to -\infty$ as $r \to 0$; we replace $r = 0$ by $r = r_0$, where r_0 is small compared with the minimum separation employed in the actual measurements. The other boundary conditions follow by simple substitution.

(a) on $y = z_a^{2/3}$, $g \leqslant 0$, $\quad U = U_s(r, z_a)$;

(b) on $y = 0$, $\quad g > 0$, $\quad \dfrac{\partial U}{\partial y} = 0$;

(c) on $y = H^{2/3}$, $\quad\quad\quad U = U_0(r, H)$;
(d) on $g = 0$, $\quad y \leqslant z_a^{2/3}$, $\quad U = U_s(r_a, z)$;

(e) on $g = \ln \dfrac{r_0}{r_a}$, $y > z_a^{2/3}$, $\quad \dfrac{\partial U}{\partial g} = 0$;

(f) on $g = g_1$, $\quad\quad\quad\quad U = U_1(r_1, z)$.

With these transformations, the differential equation (A5) becomes

$$\frac{\exp(-2g)}{r_a^2} \frac{\partial^2 U}{\partial g^2} + \frac{4}{9} y^{-1} \frac{\partial^2 U}{\partial y^2} - \left[\frac{2}{3} y^{-\frac{1}{2}} \frac{d(\ln \rho)}{dz} + \frac{2}{9} y^{-2}\right] \frac{\partial U}{\partial y} = 0.$$

The quantity $d(\ln \rho)/dz$ is left untransformed to indicate that it is calculated as a function of z.

The numerical calculations leading to the models presented in this paper were carried out on a 50×75 grid, with $r_0 = 0.1$ m, $r_1 = 10$ km, and grid spacings $\delta g = \ln 0.1$ and $\delta y = H^{2/3}/75$. The source notch size was taken to be 2×2 grid intervals, i.e. $r_a = \exp(2 \delta g)$ and $z_a = (2 \delta y)$.